PRZEGLĄD SPAWALNICTWA
Welding
TECHNOLOGY REVIEW

DOI: http://dx.doi.org/10.26628/wtr.v91i12.1084

Article

Condition monitoring of crack extension in the reinforced adhesive joint by carbon nanotubes

Omid Sam-Daliri[1], Mohammadreza Farahani[1] and Alireza Araei[1,*]

[1] School of Mechanical Engineering, College of Engineering, University of Tehran, Iran
Ph. D. Omid Sam-Daliri, email: Omid_sam@ut.ac.ir;
Prof. Mohammadreza Farahani, mrfarahani@ut.ac.ir;
* Correspondence: Prof. Alireza Araei, alaraee@ut.ac.ir

Received: 02.09.2019; Accepted: 12.11.2019

Abstract: Carbon nanotubes (CNT) are ideally suited to be employed for damage sensing in fiber reinforced composite structures. In this work, the capability of CNTs for crack extension of a single lap Al-Al adhesive joints (SLJ) under shear load is studied using electrical resistance change. Different weight percent of CNT are added to epoxy adhesive. Epoxy adhesive with high concentration of CNT is obtained during shear loading to have the maximum strength and provide the best sensory properties. To provide a more concise evaluation of the crack extension in the adhesive layer under shear load, artificial defects are embedded into the SLJ specimens. The effects of square and circular defects with two different sizes on the crack extension in the adhesive layer are evaluated. The results showed that the maximum relative resistance change has occurred by 220% when the microcracks are initiated and accordingly developed from the nanoadhesive and changed its direction from the Square defect boundary. Additionally, in comparison with interface fracture in defective adhesive joint, when a part of crack grows through the adhesive layer, the resistance change showed higher values.

Keywords: carbon nanotubes; single lap adhesive joint; damage sensing; electrical resistance change

Introduction

Adhesive joints are employed in manifold areas such as automotive, marine, aircraft, and oil and gas industry. These applications profit from the advantages of adhesive joints, such as less weight, even distribution of the load path and decreased stress concentration compared to, e.g., fastening and welding joints. However, easy inspection of adhesive joints is often only possible in a destructive way. Nondestructive inspection requires more elaborate methods and strategies. Recent research addresses NDT approaches for damage detection in adhesive joints. Michaloudaki et al. [1] detect artificial imperfections in adhesive joint by the neutron radiography method. Ren et al. [2] study adhesive defects between composite laminates using ultrasonic guided wave technique. Palumbo et al. [3] study debonding in adhesive composite joints by lock-in thermography and ultrasonic C-scan imaging. Croccolo et al. [4] use acoustic emission as condition monitoring technique for the evaluation of defect densities in adhesive bonding to predict the actual failure load of the adhesive joint. Some of these techniques, like acoustic emission are online methods for determining the damage progression in bonded joints and composites as reported by Cawley [5] and De Freitas [6] respectively. Such online methods enable to predict the onset and progression of damage under the mechanical load.

In this context, Multi-Wall Carbon NanoTubes (MWCNTs) with distinctive mechanical and electrical properties can be employed to strengthen, but also monitor the joints condition. Thostenson et al. [7] study the tensile behavior of CNT-epoxy nanocomposite films. The authors report that, by adding the carbon nanotubes to the polyester matrix, the tensile modulus, yield strength and ultimate strength of the final polymer films are increased. Li et al. [8] reached an improvement in electrical properties of CNT-epoxy nanocomposite by surface treatment of the carbon nanotube specimens. These properties build the foundation to use carbon nanotubes dispersed in epoxy as in-situ sensors for many applications. The electrical resistance of the MWCNT-epoxy nanocomposite sensor changes under applied mechanical stress. The changes in electrical resistance result from deformation and damage progression in the polymer composite structures. Based on the changes in electrical resistance, Kwon et al. [9] use several MWCNT thin films for damage sensing in Carbon fiber epoxy composites. In further studies, MWCNT- epoxy

nanocomposite are used for damage sensing by analyzing the changes in electrical resistance [10,11]. These sensory features of MWCNT-epoxy nanocomposites are exploited to use these nanocomposites as strain sensors for health monitoring in industry [12,13,14,15].

The present work studies the sensory capabilities of the defective single lap CNT-epoxy adhesive joints under quasi-static loading conditions using an Alternating Current (AC) stimulus. For comparison, different weight percentages of MWCNT are added to the adhesive layer. The electrical resistance response of the adhesive joints is then measured during shear loading. Furthermore, the microstructure of the fracture surface of the adhesive layer is evaluated by Scanning Electron Microscopy (SEM) to infer a correlation between the microstructure and forming of the conductive networks in the adhesive layer. Then, several square and circular defects were embedded in the adhesive layer to analyse their influence on the damage progression in the electrical resistance response during the shear load.

Materials, Specimens Preparation and Measurement Methods

Materials and specimens preparation

The prepared nanoadhesive contains epoxy as the matrix and MWCNTs as the conductive nanofiller. The employed epoxy resin is EpoThin® (Buehler, Germany) which is a free flowing, low viscosity, low shrinkage epoxy resin which allows the nanofiller to easily distribute in the EpoThin matrix. It has a typical cure time of nine hours at 27 °C or can be kept at room temperature for 24 hours according to the manufacture datasheet. It is provided by Buehler Company. MWCNTs nanoparticles by Cheaptube (USA) are used in this study. The outer diameter of the employed MWCNT is d_p = 30 to 50 nm. The length of the used MWCNT is between l_p = 10 to 20 μm with a purity more than 95%. Type 5754 (Al-Mg3) aluminum plates are used as adherents for the single lap adhesive joints. These adherends are manufactured according to the ASTMD5868-01 standard with a thickness t = 3 mm, length L_a = 102 mm, and width w = 25 mm. Mechanical properties of the Al adherent according to the manufacturer data sheet (Cut-Cut Corporation in Salzburg) are given in table I.

Table I. Mechanical properties of Al-Mg3

Poisson's ratio	Elastic modulus	Ultimate strength	Yield strength
0.33	68 (GPa)	330 (MPa)	280 (MPa)

Weighed amounts of epoxy resin and MWCNT (measured by a digital scale with accuracy equal to 0:0001 g) are mechanically stirred for t_s = 5 min in a beaker. The mixture was then placed in a shear mixer (IKA T18 digital ULTRA TURRAX) at 1000 rpm for t_m = 15 min. Then, the dispersion of the MWCNT in the epoxy resin is further aided using a sonication bath. A sonication bath with high frequency (f_b = 35÷60 kHz) is used to disperse the MWCNT in the epoxy resin appropriately and break the agglomerated particles. Weight percentages of 2.5, 6 and 9 wt.% MWCNTs are added to the epoxy resin [16]. Then the obtained material was mixed with a hardener in the ratio of 2:1 for t_h = 15 min on the stirrer and was immediately poured into the SLJ molds. Internal surfaces of the mold are covered with RENLEASE QV 5110 wax to ensure that no bond is formed between the Al adherents and the molds. The molds are designed so that the thickness of the adhesive layer is t_a = 1 mm for all specimens. The adhesive layer further covers a length L = 30 mm. In order to assess the effects of macroscopic defects on the impedance response of the SLJs, defects of different sizes and shapes are embedded in the center of the adhesive layer. The defects are prepared from rubber with t_d = 1 mm thickness. The outer surface of the defect is also covered by wax to prevent bonding between the nanoadhesive and the defects. After 24 h, the SLJ samples are extracted from the mold. The SLJs during and after preparation are shown in figure 1 respectively. Non-conductive end tabs are attached to the adherents to make an alignment in the universal tensile machine so that the center line of the upper and lower tabs pass through the middle of the adhesive [17], as well as to electrically isolate the specimens from the tensile test machine. In order to measure the electrical properties of the specimens, metallic wires are attached to the specimens using conductive copper adhesive. In order to also analyze the effects of defective adhesive joints, defects were added to the adhesive layers, both of square or circular shape and with different size. The defect shapes and sizes chosen in this study are given in table II.

Table II. Size and shape of 3D defects

Defect shape	Defect area/overlap area [%]	Defect size [mm]
Circular	10, 30	Radius: 4.88, 8.46
Square	10, 30	Length: 8.66, 15

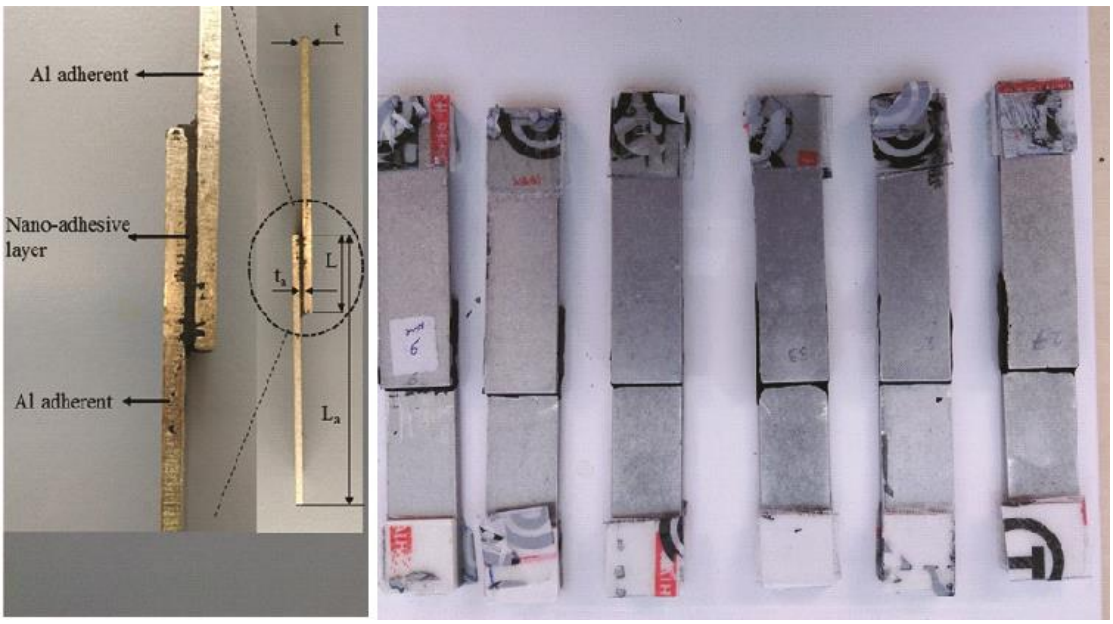

Fig. 1. Single lap adhesive joint: a) fabrication set up, b) preparation and c) specimens

Mechanical and Electrical Acquisition System

The effects of various filler contents are investigated on the initial equivalent parallel resistance (R_P) of the adhesive joint. Then, the specimens were subjected to a shear load until fracture using a Zwick/Roell Z020 universal testing machine. A crosshead displacement rate of d_r = 1 mm/min is applied [9,18,19]. The tensile force, longitudinal displacement and voltage changes versus time are measured concurrently.

The electrical measurements are conducted in two steps. In the first step, the frequency dependent initial resistance of the specimens is determined using an LCR measurement bridge by Extech Instruments. This instrument determines the equivalent parallel resistance (indicated by R_P in table III) at different frequency settings. This is done assure suitable resistance values and to determine a suitable frequency for the subsequent tensile testing. The second step is the electrical resistance change during tensile loading. These measurements are done using a high-speed, high-resolution measurement platform [20]. The electro-mechanical measurement setup is demonstrated in figure 2, the SLJ-specimen in tensile test machine is connected to the input analog amplifier chain as part of the electrical resistance change hardware. The output of the measurement hardware, applying a digitally generated sine signal. In the digital domain, the measurement platform also provides the algorithms necessary for signal processing, e.g. down-conversion of the acquired signal. Through the preliminary analysis, the measurements frequency is chosen to be f_m = 5 kHz with an excitation voltage of u_e = 1 V (signal generator in Fig. 2). Via the shunt resistance of r_s = 50 Ω, a voltage reading is recorded which is proportional to the resistance of the sample.

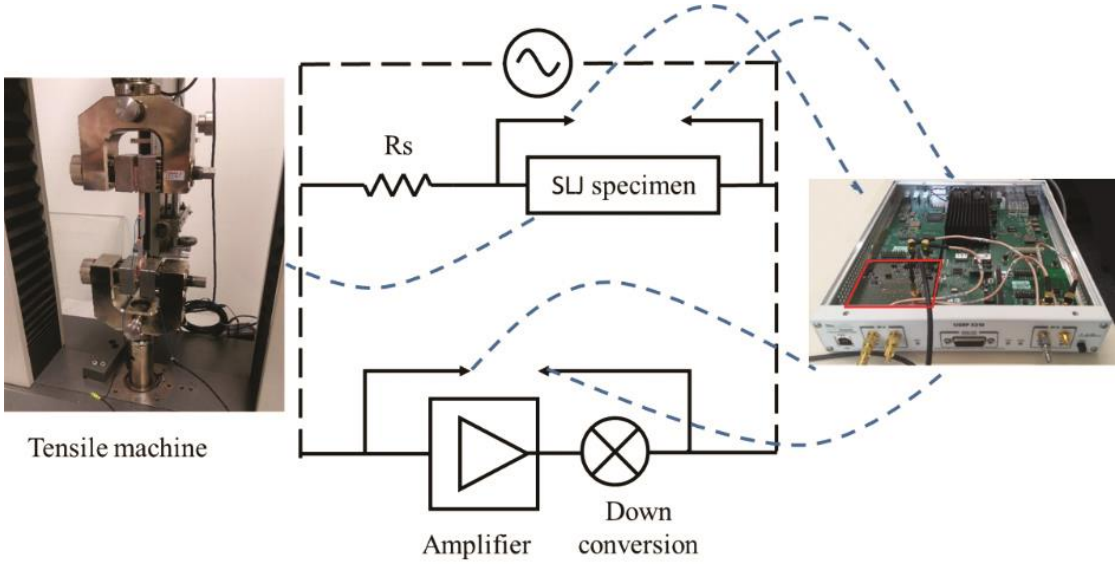

Fig. 2. Illustration of the electrical resistance change setup during the tensile test

Results and Discussion

Morphology

Prior to investigate the electromechanical behavior and crack extension, it is necessary to get a deeper understanding about the MWCNT distribution into the adhesive layer. Figure 3 shows the SEM pictures obtained from the fracture surface of MWCNT-epoxy nanocomposite containing 9 wt.% MWCNT. The MWCNTs distributed in epoxy matrix randomly which contributes in creation of conductive paths in epoxy adhesive. As reported by Ning Hu et al. [21], for a system made of conductive fillers inside an insulating matrix, tunneling effect between neighboring nanomaterials or clusters and contact mechanism between the clusters were the main conductivity mechanisms. According to SEM images, in MWCNT-epoxy composite, tunneling effect between clusters or neighboring CNTs and contact resistance are the dominant mechanisms of conductivity.

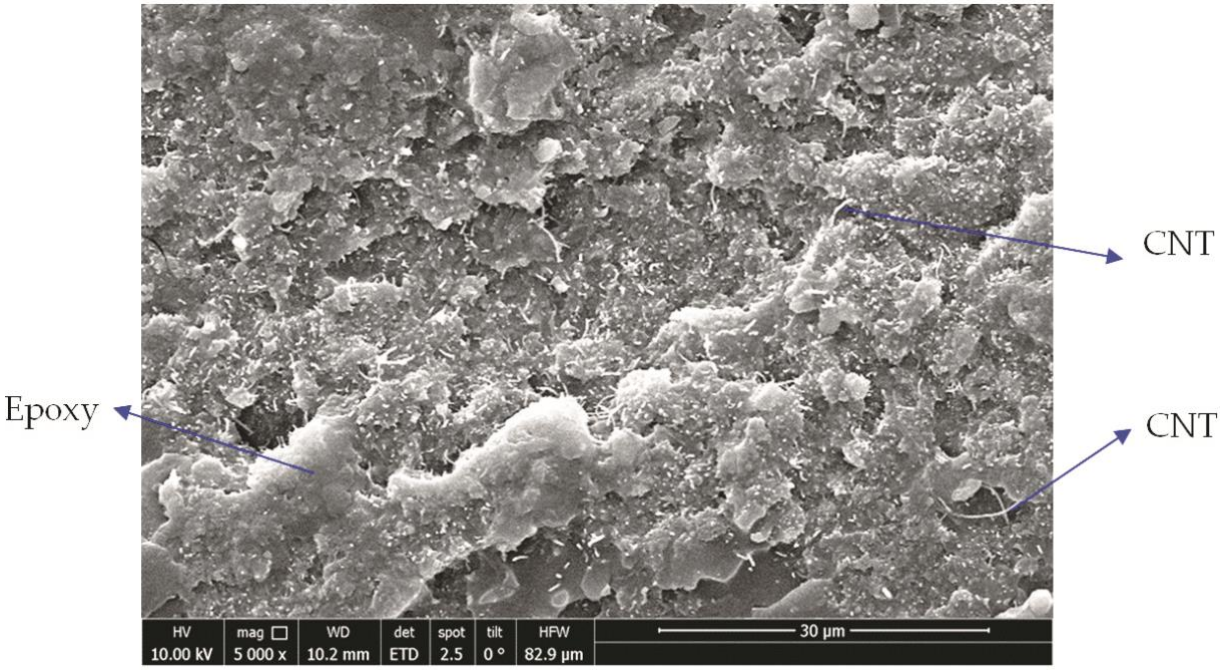

Fig. 3. Fracture surface images of MWCNT – epoxy nanocomposite with 9 wt.% MWCNT with magnification of 5 kx (kx indicates a factor of 1000)

Effect of Applied Frequency on Equivalent Parallel Resistance

The equivalent parallel resistance of the adhesive joint changes significantly when measuring at different frequencies using the LCR meter. As depicted in table III, the values of R_P, which is the equivalent parallel resistance, for 2.5 wt.% of MWCNT at different frequencies are significantly above 1 MΩ and the resistance changes between the lowest and highest frequencies is r_c = 55.31 MΩ. For condition monito ing of the adhesive joint under shear load, it is necessary to select the proper frequency based on the resistance value of the adhesive layer so that the resistance change reading is adjusted accordingly. At higher frequencies, a pre-dominant capacitive effect can be observed (the same as occurs in insulators). This effect can be used to increase the signal strength of the measurement signal. Consequently, we applied a 100 kHz excitation signal for specimens with lower concentration of CNT (2.5 and 6 wt.%) as well as 5 kHz for specimens with 9 wt.% CNT. We could thus reach measurement signals in the same range.

The tensile test results of the SLJs with different contents of MWCNT are shown in figure 4. Obviously, the increase in the concentration of MWCNTs from 2.5 to 9 wt.% results in a further increase in the bond strength.

Table III. Equivalent parallel resistance for a single lap adhesive joint at different frequencies

Adhesive layer properties	R_P (MΩ) at f_1=100 Hz	R_P (MΩ) at f_2=1 kHz	R_P (MΩ) at f_1=5 kHz	R_P (MΩ) at f_3=10 kHz	R_P (MΩ) at f_4=100 kHz	r_c (MΩ) between f_1 and f_4
2.5 wt. % CNT-epoxy	59 E+00	14.8 E+00	11.04 E+00	7.38 E+00	3.69 E+00	55.31 E+00
6 wt. % CNT-epoxy	0.970 E+00	0.412 E+00	0.402 E+00	0.367 E+00	0.150 E+00	0.82 E+00
9 wt. % CNT-epoxy	1.576E-03	0.895E-03	0.763 E-03	0.634E-03	0.523E-03	1.053 E-03

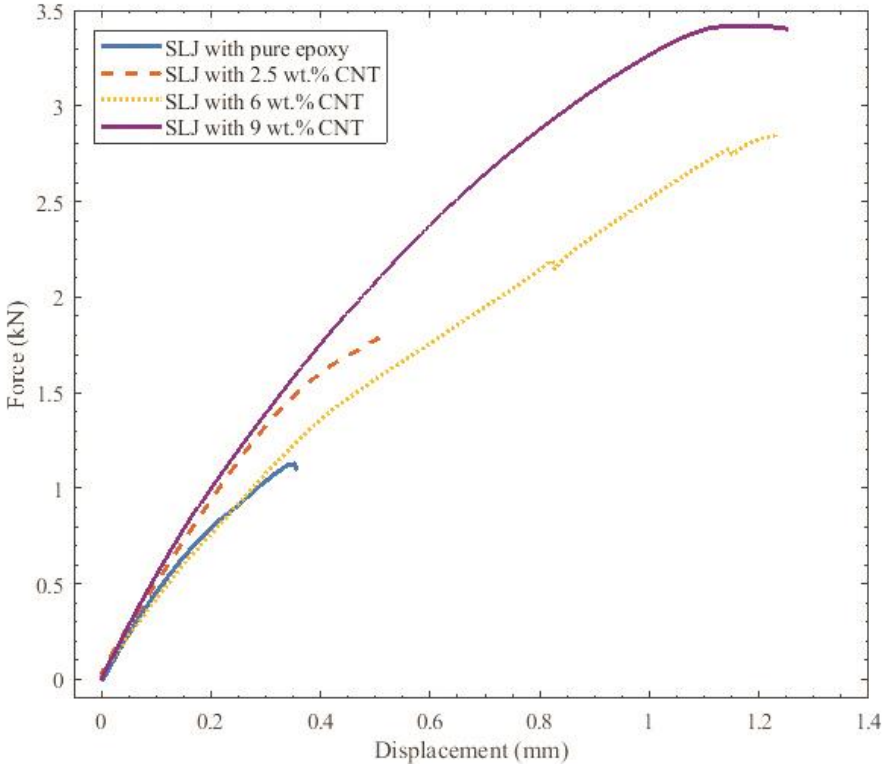

Fig. 4. Force-displacement graphs of single lap adhesive joints with different concentration of CNT

Effect of MWCNT Weight Percent on Sensing Properties

The influence of different weight percent of MWCNT on the electrical resistance response of the SLJ together with the results of the tensile test are shown in figure 5. Since the experimental results were at the same ranges, and the result scatters were less than 5%, only the averages of the results are presented. In these diagrams, the axes giving the impedance changes are plotted at different scales as the impedance changes are at different ranges. The changes in resistance result from the promotion of shear deformation in the adhesive layer.

As mentioned in section 3.2, a measurement frequency of f_m = 100 kHz is applied for specimens with lower conductivity (2.5 and 6 wt.% of MWCNT) (Fig. 5a and 5b), and f_m = 5 kHz was used for the specimens with higher conductivity (9 wt.%) (Figure 5c).

For the specimens with 2.5 wt.% filler concentration, the starting point of a sharp increase of the relative resistance change (ΔR/R) occurs at a shear displacement d = 0.35 mm, where at a shear load F of the 80% maximum force F_{max}, i.e. F/F_{max} = 80%, ΔR/R increases by 20% (from 0% to 20%) (Figure 5a). A sharp increase in resistance occurs when a crack extension is initiated. A progressive increase in the slope of the resistance curve can not be observed at further extension of the crack (0.35 mm < d < 0.52 mm). Consequently, these specimens are only applicable for the evaluation of the large crack growth in the adhesive joint (Figure 5a). The resistance increase here may result from growing primary microcracks in the epoxy matrix which remain from the preparation. Such a phenomenon of resistance increase due to microcrack extension in composite structures is already described by Thostenson et al. [22].

Figure 5b shows the electro-mechanical results of the specimens containing 6 wt.% of MWCNT in the adhesive layer. The sharp increase in the resistance curve due to primary microcracks occurs at d = 1.075 mm and F/F_{max} = 95%. In the progression from the first cracking to the ultimate failure point, the resistance change increases continually. This results from the accumulation of the microcracks, here the change of ΔR/R = 1 to 1.8% (see Fig. 5b). Thus, these specimens are more sensitive to a damage progression in adhesive layer.

The electrical resistance response of the adhesive joint during shear loading for the specimen with 9wt.% of MWCNT is shown in figure 5c. There is a quasi-linear increase in resistance change from initial loading until the large step increase of ΔR/R = 4% at d= 0.9 mm. There is also a further increase in ΔR/R for d > 0.9 mm, corresponding to the increase of damage accumulation. The changes in slope of ΔR/R is large relative to the other specimens (2.5 and 6wt.%). Therefore, it is possible to identify the nature and damage extension in adhesive layer using the specimens with 9 wt.% MWCNT.

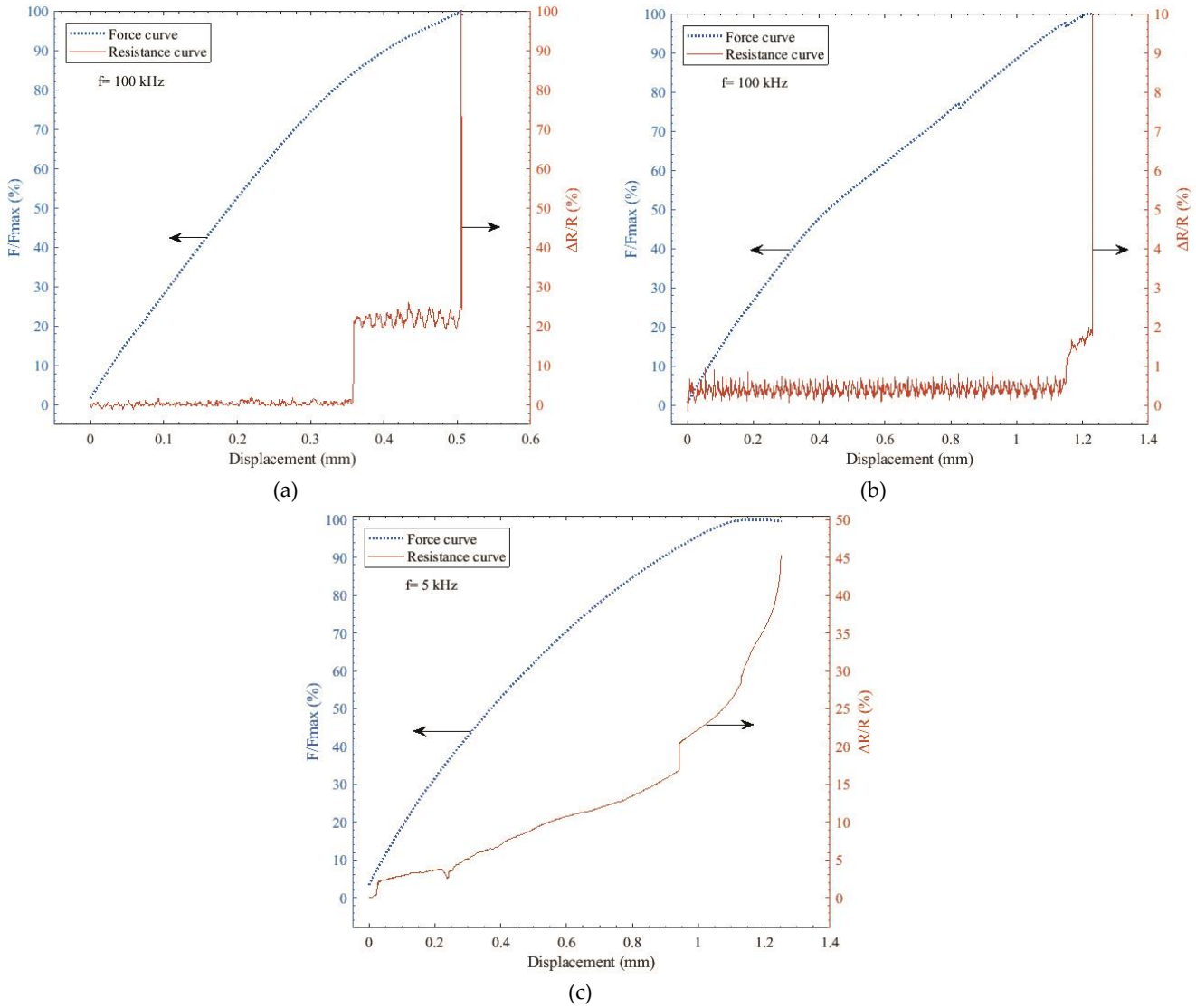

Fig. 5. Mechanical and electrical resistance response of SLJ with different weight percent of MWCNT: a) 2.5 wt.%, b) 6 wt.%, c) 9 wt.%. The arrows indicate the axis belonging to the respective curve.
Note: the scaling on the right-hand axis and displacement below are not uniform throughout the illustrated results

Effect of the Artificial Defects on the Sensitivity

The nature and propagation of damage in the adhesive layer with embedded defects are assumed to be the same as in adhesive joints without embedded defects [18]. The electro-mechanical behavior and fracture surface of the adhesive joints with a_d = 10 % embedded defect area, including circular and square defects in the adhesive layer, are shown in figures 6a and 6b, respectively. It can be seen from figure 6a that crack progression continued in the adhesive layer without an extension into the circular defect boundary. We may assume that, when there is a continuous crack growth in adhesive layer, the electrical resistance response increases quasi-linearly from the starting point of shear loading until ultimate fracture without constant segments in the resistance change. The results in figure 6b, let assume that there is no crack propagation in the adhesive layer, i.e. the crack extension occurs from the interface between the adhesive layer and metal adherent. Consequently, there is no quasi-linear behavior in the resistance change for the large part of the shear displacement (d < 0.63 mm). Furthermore, the electrical resistance response in figure 6b shows that accumulation of microcracks and damage progression in the specimens start at d = 0.63 mm. The impedance result shown in figure 6a is very similar to the specimens without artificial defects (compare Fig. 5c). A possible explanation could be that in both of the specimens, the fracture behavior occurs in the adhesive layer. Another reason could be that the specimens have nonzero slope in the ΔR/R from the initial loading until ultimate fracture.

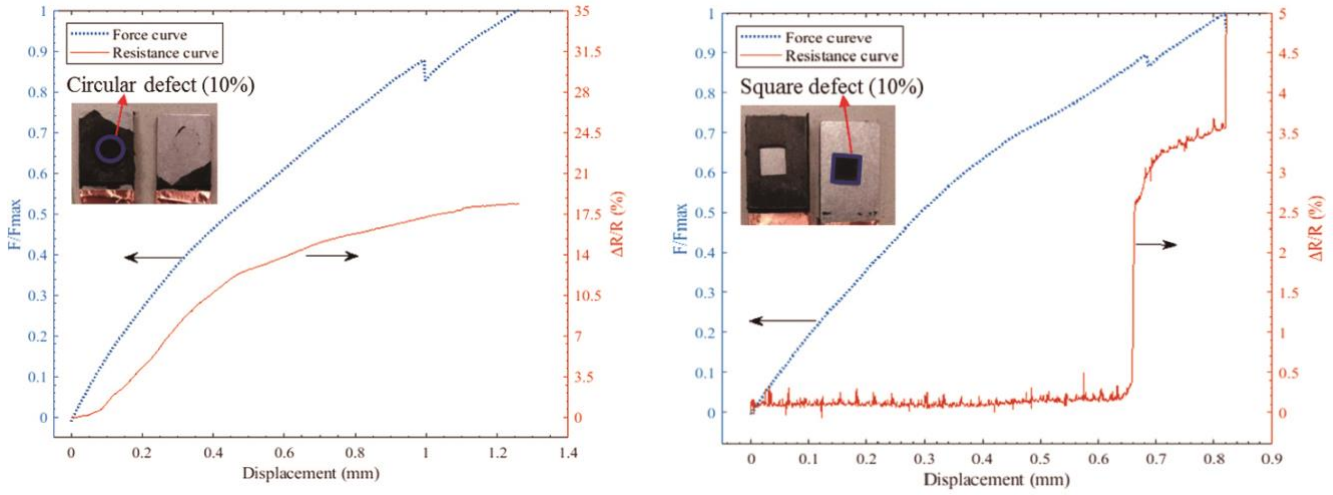

Fig. 6. Mechanical and electrical resistance response of SLJ including observed fracture surface with: a) 10% circular defect area and b) 10% square defect area. The arrows indicate the axis belonging to the respective curve.
Note: the scaling on the right-hand axis and displacement below are not uniform throughout the illustrated results

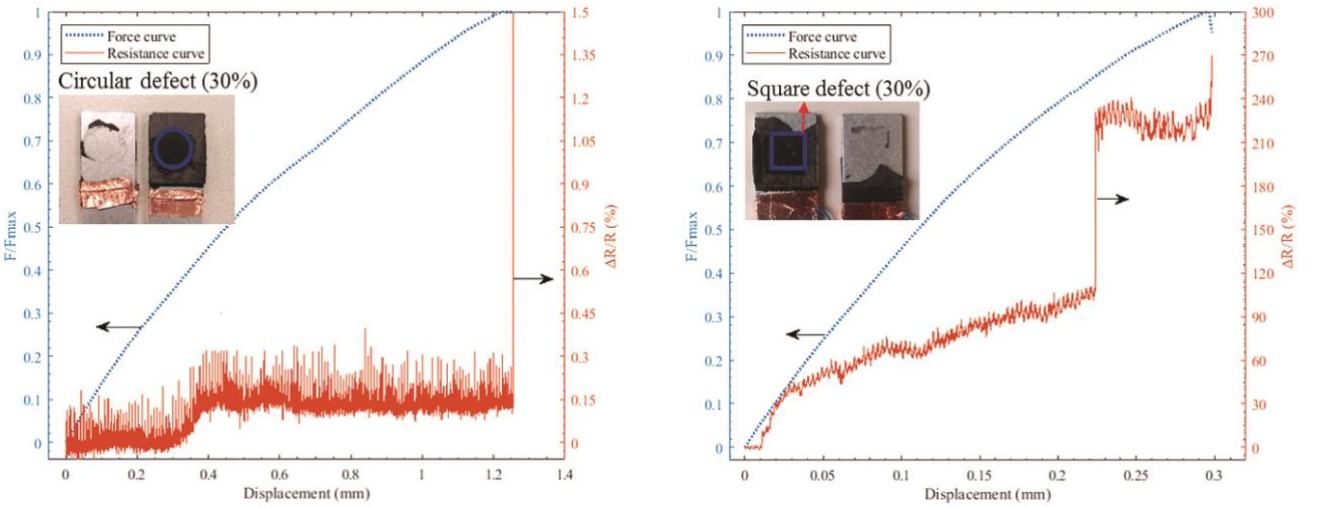

Fig. 7. Mechanical and electrical resistance response of SLJ including observed fracture surface with: a) 30% circular defect area and b) 30% square defect area. The arrows indicate the axis belonging to the respective curve.
Note: the scaling on the right-hand axis and displacement below are not uniform throughout the illustrated results

Impedance results for defects with 30 % of overlap area in circular and square shape, embedded in adhesive layer, are shown in figure 7a and 7b, respectively. In figure 7a, since the fracture is occurred from the interface between the adhesive and substrate, the total increase in ΔR/R showed a small value (ΔR/R = 0.15%). From figure 7b we may assume that the cracks in the adhesive layer initiate at and reach from the defect boundary. In this situation the direction of the crack extension is changed and one sharp resistance change occurs at d = 0.23 mm (ΔR/R = 100% to 220%). Consequently, we may conclude that the both shape and size of defect are influence on the electrical resistance response, and the change of ΔR/R is also related to the crack extension in adhesive layer. For a larger size of the defects with square shape, the crack extends from in adhesive and reach to defect boundary. Therefore, it showed the maximum amount in ΔR/R.

Conclusions

The presented study focuses on the condition monitoring capabilities of SLJs using conductive nanoadhesive. Conductive nanoadhesive was prepared with different filler contents of MWCNT (2.5, 6 and 9 wt.%). The capability of the prepared MWCNT-epoxy SLJs as nanocomposite sensors for adhesive joints

was studied by determining their electrical impedance changes during loading. The best damage sensing capabilities of the adhesive joint were identified for specimens with 9 wt.%. The sensitivity of the conductive nanoadhesive was studied for defective adhesive joints with defects of 10 and 30% overlap area shapes. The results showed that damage progression in adhesive joints depends on the behavior of the crack growth in the adhesive layer and geometrical properties of the defect. Embedded larger sizes of defects with square shape indicated the most changes in electrical resistance by 220% because the crack has initiated and developed from the adhesive and its direction is changed from the defect boundary.

Author Contributions: O.S.-D. prepared the specimens, contributed to electrical and mechanical testing, did the analysis in MATLAB, drafted and edited the prepared. M.F. and A.A. reviewed the paper and provided supervision.

Funding: This research received no external funding.

Acknowledgments: This study was financially supported by The Welding and Non Destructive Testing Applied Research Center (TWN), University of Tehran. Additionally, the preparation of specimens, mechanical testing equipment were supplied by TWN.

Conflicts of Interest: The authors declare no conflict of interest.

References

[1] Michaloudaki M., Lehmann E., Kosteas D., Neutron imaging as a tool for the non-destructive evaluation of adhesive joints in aluminium, *International Journal of Adhesion and Adhesives*, 2005, vol. 25(3), 257-267. [CrossRef]

[2] Ren B., Lissenden C. J., Ultrasonic guided wave inspection of adhesive bonds between composite laminates, *International Journal of Adhesion and Adhesives*, 2013, vol. 45, 59-68. [CrossRef]

[3] Palumbo D., Tamborrino R., Galietti U., Aversa P., Tati A., Luprano V., Ultrasonic analysis and lock-in thermography for debonding evaluation of composite adhesive joints, *NDT & E International*, 2016, vol. 78, 1-9. [CrossRef]

[4] Croccolo D., Cuppini R., Adhesive defect density estimation applying the acoustic emission technique, *International Journal of Adhesion and Adhesives*, 2009, vol. 29(3), 234-239. [CrossRef]

[5] Cawley P., Adams R., Defect types and non-destructive testing techniques for composites and bonded joints, *Materials Science and Technology*, 1989, vol. 5(5), 413-425. [CrossRef]

[6] De Freitas S. T., Zarouchas D., Poulis J., The use of acoustic emission and composite peel tests to detect weak adhesion in composite structures, *The Journal of Adhesion*, 2018,vol. 94(9), 743-766. [CrossRef]

[7] Thostenson E. T., Chou T.-W., Aligned multi-walled carbon nanotube-reinforced composites: processing and mechanical characterization, *Journal of Physics D: Applied Physics*, 2002, vol. 35(16), L77. [CrossRef]

[8] Andalib H., Farahani M., Enami M., Study on the new friction stir spot weld joint reinforcement technique on 5754 aluminum alloy, *Proceedings of the Institution of Mechanical Engineers, Part C: Journal of Mechanical Engineering Science*, 2018, vol. 232(17), 2976-2986. [CrossRef]

[9] Kwon D.-J., Wang Z.-J., Choi J.-Y., Shin P.-S., DeVries K. L., Park J.-M., Damage sensing and fracture detection of CNT paste using electrical resistance measurements, *Composites Part B: Engineering*, 2016, vol. 90, 386-391. [CrossRef]

[10] Na W.-J., Byun J.-H., Lee M.-G., Yu W.-R., In-situ damage sensing of woven composites using carbon nanotube conductive networks, *Composites Part A: Applied Science and Manufacturing*, 2015, vol. 77, 229-236. [CrossRef]

[11] Sam-Daliri O., Faller L.-M., Farahani M., Roshanghias A., Oberlercher H., Mitterer T., et al., MWCNT–Epoxy Nanocomposite Sensors for Structural Health Monitoring, *Electronics*, 2018, vol. 7(8), 143. [CrossRef]

[12] Ahmed S., Schumacher T., McConnell J., Thostenson E. T., Experimental and Numerical Investigation on the Bond Strength of Self-Sensing Composite Joints, *International Journal of Adhesion and Adhesives*, 2018, vol. 84, 227-237. [CrossRef]

[13] Kang I., Schulz M. J., Kim J. H., Shanov V., Shi D., A carbon nanotube strain sensor for structural health monitoring, Smart materials and structures, 2006, vol. 15(3), 737. [CrossRef]

[14] O. Sam-Daliri, L.-M. Faller, M. Farahani, A. Roshanghias, A. Araee, M. Baniassadi, *et al.*, Impedance analysis for condition monitoring of single lap CNT-epoxy adhesive joint, *International Journal of Adhesion and Adhesives*, 2019, vol. 88 59-65.

[15] C. Stetco, O. Sam-Daliri, L.-M. Faller, and H. Zangl, "Piezocapacitive Sensing for Structural Health Monitoring in Adhesive Joints," in *2019 IEEE International Instrumentation and Measurement Technology Conference (I2MTC)*, 2019, pp. 1-5.

[16] Georgousis G., Pandis C., Kalamiotis A., Georgiopoulos P., Kyritsis A., Kontou E., et al., Strain sensing in polymer/carbon nanotube composites by electrical resistance measurement, *Composites Part B: Engineering*, 2015, vol. 68, 162-169. [CrossRef]
[17] Nunes L., Mechanical characterization of hyperelastic polydimethylsiloxane by simple shear test, *Materials Science and Engineering: A*, 2011, vol. 528(3), 1799-1804. [CrossRef]
[18] O. Daliri, M. Farahani, and M. Farhang, A combined numerical and statistical analysis for prediction of critical buckling load of the cylindrical shell with rectangular cutout, *Engineering Solid Mechanics*, 2019, vol. 7 *(1)*, 35-46.
[19] O. Sam Daliri and M. Farahani, Characterization of Stress Concentration in Thin Cylindrical Shells with Rectangular Cut-out Under Axial Pressure, *International Journal of Advanced Design and Manufacturing Technology*, 2017, vol. 10(2), 133-141. [Hyperlink]
[20] Faller L.-M., Mitterer T., Leitzke J. P., Zangl H., Design and Evaluation of a Fast, High-Resolution Sensor Evaluation Platform Applied to MEMS Position Sensing, *IEEE Transactions on Instrumentation and Measurement*, 2017, vol. 67(5), 1014-1027. DOI: 10.1109/TIM.2017.2771955 [Hyperlink]
[21] Hu N., Karube Y., Yan C., Masuda Z., Fukunaga H., Tunneling effect in a polymer/carbon nanotube nanocomposite strain sensor, *Acta Materialia*, 2008, vol. 56(13), 2929-2936. [CrossRef]
[22] Thostenson E. T., Chou T. W., Carbon nanotube networks: sensing of distributed strain and damage for life prediction and self healing, *Advanced Materials*, 2006, vol. 18(21), 2837-2841. [CrossRef]